ACS APPLIED MATERIALS & INTERFACES

Research Article

Cite This: ACS Appl. Mater. Interfaces 2018, 10, 9069−9076

www.acsami.org

Exploration of Ultralight Nanofiber Aerogels as Particle Filters: Capacity and Efficiency

Fabian Deuber,[†] Sara Mousavi,[†,‡] Lukas Federer,[†] Marco Hofer,[§] and Christian Adlhart*[,†]

[†]Institute of Chemistry and Biotechnology, Zurich University of Applied Sciences ZHAW, Einsiedlerstrasse 31, 8820 Wädenswil, Switzerland

[‡]Department of Chemical Engineering, University of Sistan and Baluchestan, University Boulevard, P.O. Box 98155-987, Zahedan, Iran

[§]Incident Response and Individual Protection Branch, Federal Office for Civil Protection, Labor Spiez, Austrasse, 3700 Spiez, Switzerland

Supporting Information

ABSTRACT: Ultralight nanofiber aerogels (NFAs) or nanofiber sponges are a truly three-dimensional derivative of the intrinsically flat electrospun nanofiber mats or membranes (NFMs). Here we investigated the potential of such materials for particle or aerosol filtration because particle filtration is a major application of NFMs. Ultralight NFAs were synthesized from electrospun nanofibers using a solid-templating technique. These materials had a tunable hierarchical cellular open-pore structure. We observed high filtration efficiencies of up to 99.999% at the most penetrating particle size. By tailoring the porosity of the NFAs through the processing parameters, we were able to adjust the number of permeated particles by a factor of 1000 and the pressure drop by a factor of 9. These NFAs acted as a deep-bed filter, and they were capable of handling high dust loadings without any indication of performance loss or an increase in the pressure drop. When the face velocity was increased from 0.75 to 6 cm s^{-1}, the filtration efficiency remained high within a factor of 1.1−10. Both characteristics were in contrast to the behavior of two commercial NFM particle filters, which showed significant increases in the pressure drop with the filtration time as well as a susceptibility against high face velocities by a factor of 105.

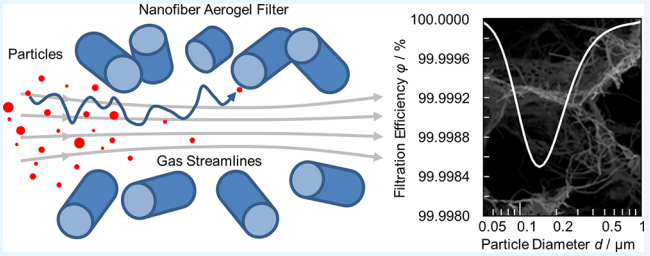

KEYWORDS: *aerosol filtration, deep-bed filtration, particle diffusion, electrospinning, sponges*

1. INTRODUCTION

Particle or aerosol filtration was one of the first applications of nanofiber mats or membranes (NFMs).[1−6] These nonwovens obtained from electrospun nanofibers with typical diameters between 50 and 1500 nm exhibit well-suited characteristics, such as relatively low air resistance, because of the gas-slip effect, as well as small pore size and high specific surface area, for efficient particle removal.[7−13] NFMs were also an integral part of the Petryanov−Sokolov particle filters that had been used in the cleanup phase of the Tschernobil site.[14,15] Later developments include multilayer setups,[16−21] and a recent approach is nanonetting, where the pores in NFMs are covered with nets of even smaller nonwoven nanofibers.[20−23] They show high filtration efficiency but also a relatively large pressure drop. When multiple electrospun mats are stacked over each other, three-dimensional (3D) filters can be obtained. The elongated flow path through the 3D construct results in higher filtration efficiency but also in higher pressure drop, as is understood empirically and by simulations.[16,17] A similar dependence of the filtration efficiency and pressure drop is found when investigating the nanofiber packing density and mat thickness.[6,24] Such NFM filters are restricting the gas flow. Furthermore, they still suffer from further significant drawbacks: inadequate filtration performance, weak mechanical properties, and short service life caused by accumulated particles on the filtration surface. The challenge, therefore, is to construct a nonwoven mat capable of outperforming common NFM filters. In our opinion, a 3D fibrous filter should meet the following criteria: (i) high filtration efficiency, but at the same time an undesirable increase in the pressure drop should be avoided; (ii) a robust and mechanical scaffold allowing easy handling; (iii) capability of handling high particle loadings and maintaining high filtration efficiency. To satisfy these requirements, we present a robust nanofiber aerogel (NFA) based on electrospun nanofibers. Our material is based on recent developments on solid-templated NFAs, where the porosity and microstructure can be tuned on a large scale.[7,25−34] We herein demonstrate the high filtration efficiency of such NFAs. The NFAs can handle very high face velocities

Received: January 9, 2018
Accepted: February 26, 2018
Published: February 26, 2018

DOI: 10.1021/acsami.8b00455
ACS Appl. Mater. Interfaces 2018, 10, 9069−9076

without significant loss of efficiency, and they show very high dust-holding capacities compared to commercial NFM filters.

2. EXPERIMENTAL DETAILS

2.1. Fabrication of NFM. The composite pullulan/poly(vinyl alcohol) (Pul/PVA) composite nanofibers were prepared by dissolving 4 g of Pul (food grade, Hayashibara Co. Ltd., Japan) and 6 g of PVA (M_w = 89000−98000 Da; DH = 99%; Sigma-Aldrich) in 90 g of water. The solution was electrospun by free surface electrospinning with a Nanospider NS Lab 500, Elmarco s.r.o. Nanofibers were spun onto baking paper at a high voltage of 80 kV using a cylindrical electrode and at a collector distance of 16 cm. The temperature and relative humidity (RH) during electrospinning were 26 ± 3 °C and 26 ± 4%, respectively. Uniform nanofibers with a diameter of 240 ± 55 nm were obtained.

2.2. Preparation of NFAs. For the NFA with an apparent density of 48.91 mg mL^{-1} and a porosity of 96.64% after thermal cross-linking, approximately 10 mg of the previously prepared NFM was cut into small pieces of approximately 1 × 1 cm^2 and dispersed in 100 mL of 1,4-dioxane. The NFM pieces were further cut and dispersed by an IKA T25 homogenizer for 20 min at 13000 rpm to obtain fibers with a fiber-length distribution of 48.8 ± 30 μm. The homogeneous dispersion was subsequently poured into a mold, degassed, and frozen at a specific rate (here 11 μm s^{-1}). The frozen solid was then freeze-dried for 48 h, and the pristine NFA was finally thermally cross-linked at a temperature of 180 °C for 40 min. Aerogels with apparent densities of 23.2 and 88.5 mg mL^{-1} and final porosities of 98.40 and 93.91% were prepared equally. NFAs with an identical apparent density of 49.1 ± 0.88 mg mL^{-1} and a final porosity of 96.85 ± 1.8% but different secondary pore sizes between 15.2 and 122.6 μm were prepared by controlling the freezing conditions. Detailed information on the fiber-length distribution after cutting and controlled freezing conditions is given in the Supporting Information of work by Deuber et al.[25,26]

2.3. Characterization. *2.3.1. Scanning Electron Micrsocopy (SEM) Images.* Cross sections of electrospun nanofiber-based aerogels were gold-coated (Quorum Q150RS sputter) for 30 s at 20 mA. SEM images of the species were then acquired using an FEI Quantum FEG250 scanning electron microscope with an acceleration voltage of 5 kV and a secondary electron detector spot size of 2.5.

2.3.2. Pore Size, Pore-Wall Thickness, and Fiber Diameter Determination. To determine the mean pore size of the final aerogels, the samples were cut perpendicularly to the freezing direction at a height of 0.5 cm. The pores were determined based on the SEM images of three cross sections by two different human operators by measuring the lengths and widths of 200 arbitrarily selected pores to obtain a mean pore size. The same procedure was applied to determine the pore-wall thickness. Fields of view of the SEM images were 800 and 400 μm, respectively.

The fiber diameter was estimated based on SEM images from the NFMs before homogenization. According to Stanger et al.,[35] each fiber was only measured once to reduce the bias for bigger fibers. Following the suggested magnification and rules for fiber diameter determination, a field of view of 3 μm was selected.[35,36]

2.3.3. Porosity of the NFA. The porosity of the NFA was determined using a standard approach for cellular materials. This method is also known as Archimedes principle:

$$\Phi = \frac{V_p}{V} \times 100\% = \frac{V - \frac{m}{\rho}}{V} \times 100\% \quad (1)$$

where Φ is the porosity, V is the total bulk volume of the aerogel, V_p is the pore volume, m is the mass, and ρ is the density of the polymeric material (40 wt % Pul, ρ = 1.85 g mL^{-1}; 60 wt % PVA nanofibers, ρ = 1.19 g mL^{-1}).

2.4. Filtration Efficiency and Filtration Behavior. To characterize the filtration behavior of the prepared NFAs, a setup for aerosol filtration constructed and validated by the Incident Response and Individual Protection Branch of Federal Office for Civil Protection was used. A certificate aerosol atomizer was used to generate di-2-ethylhexyl sebacate (DEHS) aerosol with a mass concentration of 29.0 mg m^{-3} and a count mean aerodynamic diameter of 208 nm. To analyze the particle size and distribution, an ultrahigh sensitivity aerosol spectrometer (type UHSAS) from Droplet Measurement Technologies was used.

From the original mold, which had a diameter of approximately 260 mm, NFA samples were cut into cylinders with a diameter of 60 mm and a height of 15 mm. These cylinders were taken from the center of the mold to ensure a minimal pore gradient, which could result from different temperature gradients at the edge of the mold during the freezing process. Similar to the ASTM D3574-11, the pieces were radially compressed to approximately 90% of their original surface area. To avoid edge-slipping effects, all of the edges were sealed using a regular high-vacuum lubricant. All NFAs were prepared in duplicate, and each measurement was duplicated. The filtration efficiency was studied at the following face velocities v_f: 0.75, 1.5, 3.0, and 6 cm s^{-1}.

2.5. Dust-Holding, Long-Term Filtration. The dust-holding capacity was determined using the same filtration efficiency test setup. A face velocity of 1.5 cm s^{-1} with a corresponding aerosol particle loading of 2 × 10^6 aerosol particles per second was used. Penetration measurements were conducted in a 2 min interval until either the pressure drop of the sample was too big (>2500 Pa) or a time limit of 45 min was reached. For comparison, two commercial NFMs with and without nonwoven microfiber toppings were studied under the same conditions.

3. RESULTS AND DISCUSSION

3.1. Synthesis of NFAs with Tailored Porosity. The principal processing steps for our NFAs are shown in Figure 1.

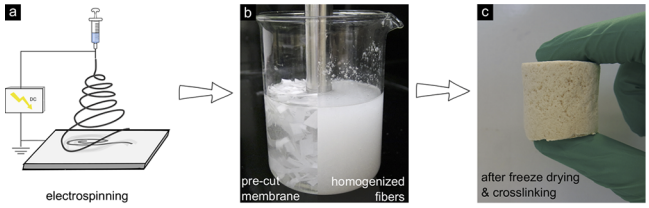

Figure 1. Main processing steps for the synthesis of a NFA: (a) fabrication of nonwoven Pul/PVA nanofibers by electrospinning; (b) cutting and homogenization of electrospun nanofibers in 1,4-dioxane using a high-speed homogenizer to obtain dispersed short nanofibers (also called slurry); (c) solid templating by freeze-drying to obtain the 3D network of short nanofibers. The pristine NFA can be postprocessed to introduce new functional groups on the fiber surface or to consolidate the structure. Using thermal cross-linking, we were able to render the fibers water-insoluble and to improve the mechanical stability of the NFA.

After electrospinning to obtain a NFM, the NFM was cut into small pieces, suspended in a wetting nondissolving liquid, and homogenized to obtain a slurry with short electrospun nanofibers. Finally, the slurry was cast into a mold and frozen at a controlled rate, and the solid-templated 3D network of short nanofibers was generated. By sublimation of the frozen nonsolvent, the freestanding NFA was obtained. Furthermore, we used a thermal cross-linking procedure to render the nanofiber polymers water-insoluble while increasing their mechanical resilience.

The freezing process of the slurry was crucial for the final architecture of the NFA: during freezing, the short nanofibers in the slurry had been rejected from the moving solidification front. Thus, the growing solvent crystals were pushing the fibers away, and thereby they created nanofiber-rich and nanofiber-sparse areas. Upon solvent removal by sublimation, only the nanofibrous skeleton was retained. The former nanofiber-rich

DOI: 10.1021/acsami.8b00455
ACS Appl. Mater. Interfaces 2018, 10, 9069−9076

areas were now the cell walls, and the large cellular pores were replicas of the solvent crystals. This natural segregation phenomenon is crucial in the freeze-casting of many different materials but was only recently used to synthesize NFAs from electrospun nanofibers.[7,27,29,33,34,37−48] Because of this effect, it was possible to tailor the architecture of the NFA. In-depth discussions for the underlying solid-templating mechanism in general[49−55] and for aerogels from electrospun fibers in particular can be found elsewhere.[26,31,37] The microscopic architecture of the aerogel revealed a hierarchical pore system, as displayed in Figure 2a,b. Larger cell-like secondary pores

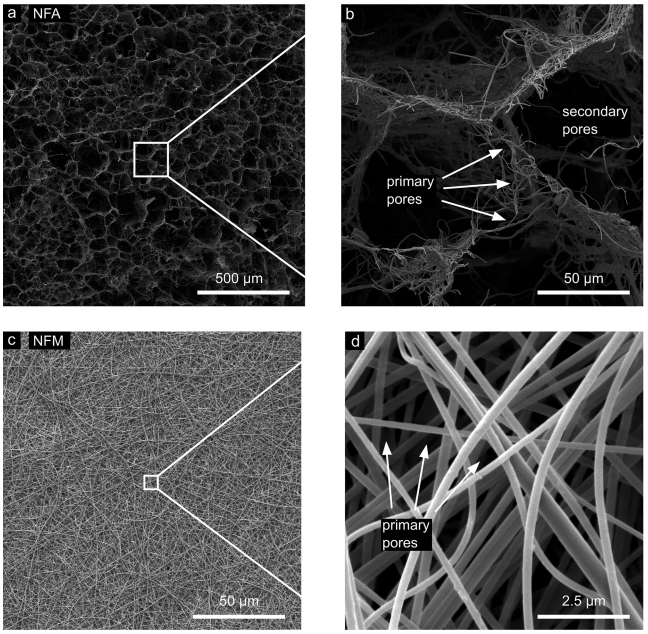

Figure 2. SEM images illustrating the morphological difference between NFAs and classical electrospun NFMs: (a) cross section and (b) close up of the NFA illustrating the hierarchical pore architecture with cells of coarse secondary pores and thin cell walls containing fine primary pores. These fine primary pores are similar in size to the pores of the electrospun NFMs (c and d), which served as the starting materials for the NFA.

were formed by freezing solvent crystals as stated above. These pores were in the range of 50−100 μm. In the close-up image of a coarse secondary pore, fine pores, between tangled nanofibers, with sizes of 2−5 μm are distinctly visible (Figure 2b). These primary pores were the same size as those for the electrospun NFM (Figure 2c,d). These primary pores interconnect the larger secondary pores, thus yielding a truly open-pore network of nanofibers with regular cellular characteristics.

By increasing the solid loading inside the slurry, it was also possible to alter the microstructure of freeze-casted structures on multiple levels. Because the solvent initially present in the slurry was converted first into a solid, which was later eliminated by sublimation to generate the porosity, the pore content could be adjusted.[53,56] Increasing the solid loading resulted in a higher volume fraction of nanofibers inside the slurry and, consequently, in a lower porosity of the NFA. Here, we produced NFAs with three different porosities: 98.40, 96.64, and 93.91%.

In contrast to the 3D NFA structure, electrospun NFMs that are applied for particle filtration are often ultrathin and show randomly deposited nanofibers (Figure 2c,d). The morphology of electrospun NFMs is also accessible from short nanofibers using a so-called wet-layering technique, as demonstrated by Greiner et al.[57,58]

3.2. Filtration Theory and Performance Evaluation.

Classical nanofibrous filters act as thin mats, which are capable of capturing small particles from an air stream. Because of their fibrous character and small porosity, even the smallest particles can be deposited on the surface of the nanofibers. This, on the other hand, leads to decreasing permeability and ultimately to a filtration failure due to high pressure. This trade-off is a very usual situation because filtering aerosol particles by fibrous filters is a complex physical process, exceeding the simple sieving principle. The filtration efficiency, φ, can be described by

$$\varphi = \frac{n_{up} - n_{down}}{n_{up}} \tag{2}$$

where n_{up} is the particle concentration before the filter and n_{down} is the particle concentration after the filter.[59,60] The filter is restricting gas flow, and the pressures before and after the filter are not the same. The pressure after the filter is lower by Δp. This is known as the pressure drop, which depends on the face velocity v_f and other parameters such as the temperature and air permeability of the filter.[59] The filtration efficiency can be used to calculate penetration of the aerosol particles through the filter. The penetration P is defined by $P = 1 - \varphi$. The dependence of P on the filter thickness and fiber diameter can be expressed by the empirical formula

$$P = \exp\left[\frac{4\alpha h}{\pi(1-\alpha)D_f}\eta\right] \tag{3}$$

where α is the filter solidity (also called the filter packing density), h the thickness of the filter, D_f the fiber diameter, and η the single fiber efficiency.[59]

The principle of particle capture by a single fiber is depicted in Figure 3a. The three major mechanisms for particle capture are by (1) diffusion, (2) interception, and (3) impact. The first mechanism—diffusion— is caused by the Brownian motion of small aerosol particles and their collision with the surface of the fiber. Increasing the internal surface of a filter by using nanofibers has a tremendous influence on diffusion-driven particle capture. Alternatively, nanofibers can be stacked on each other but at the cost of an increased differential pressure. NFAs, with their hierarchical pore structure, on the other hand, could fulfill both requirements: free air flow through the secondary pores while offering an increased internal surface through the cell walls of the nanofibers.

To simplify the complex manner of the filtration mechanism of fibrous filters, Lee and Lui[59,61] suggested a semiempirical correlation of the single fiber efficiency

$$\eta_{exp} = 2.6\left(\frac{1-\alpha}{Ku}\right)^{1/3} Pe^{-2/3} + \left(\frac{1-\alpha}{Ku}\right)^{1/3}\frac{R^2}{1+R} \tag{4}$$

where K is the Kuwabara hydrodynamic factor and Pe denotes the Peclet number, which can be calculated by $Pe = uD_p/D$. D_p is the particle diameter, u the interstitial gas velocity within the filter, and D is the diffusion coefficient of the aerosol particle. The variable R is the interception parameter ($R = D_p/D_f$). On the basis of this model, we fitted our data to the experimental filtration curves, as shown in Figure 4. By a reduction of the

DOI: 10.1021/acsami.8b00455
ACS Appl. Mater. Interfaces 2018, 10, 9069−9076

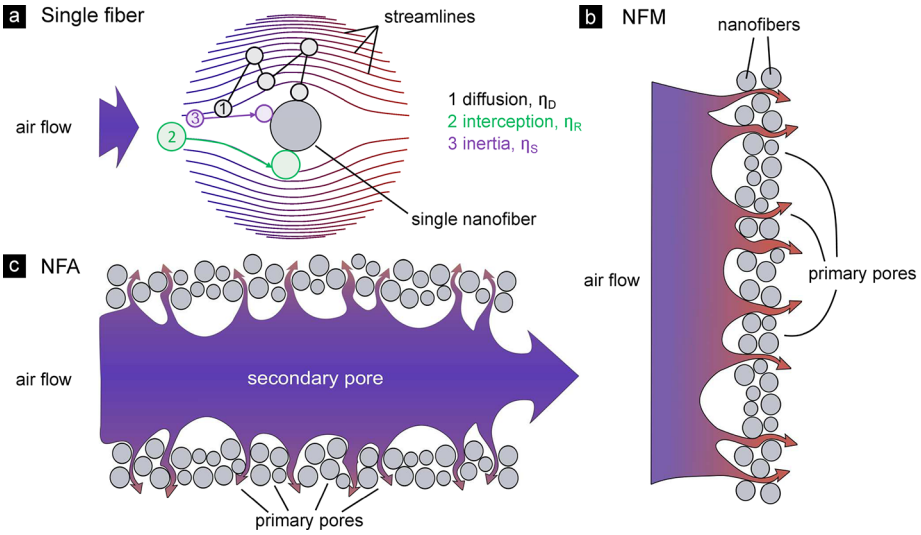

Figure 3. Schematic illustration of particle filtration mechanisms by (a) a single nanofiber, (b) a NFM, and (c) a cellular 3D NFA (c). The three major mechanisms for particle capture are by (1) diffusion, (2) interception, and (3) impact. Upon incorporation into a thin NFM (b), dead-end filtration will be applied with short diffusion times and rapid cake formation on the primary pores in the case of high particle loadings. Filtration through a NFA can be described as a kind of cross-flow filtration with large diffusion channels through the secondary pores, allowing one to reduce the pressure drop and to increase the capacity. Part a was adapted with permission from ref 58. Copyright 2016 John Wiley and Sons.

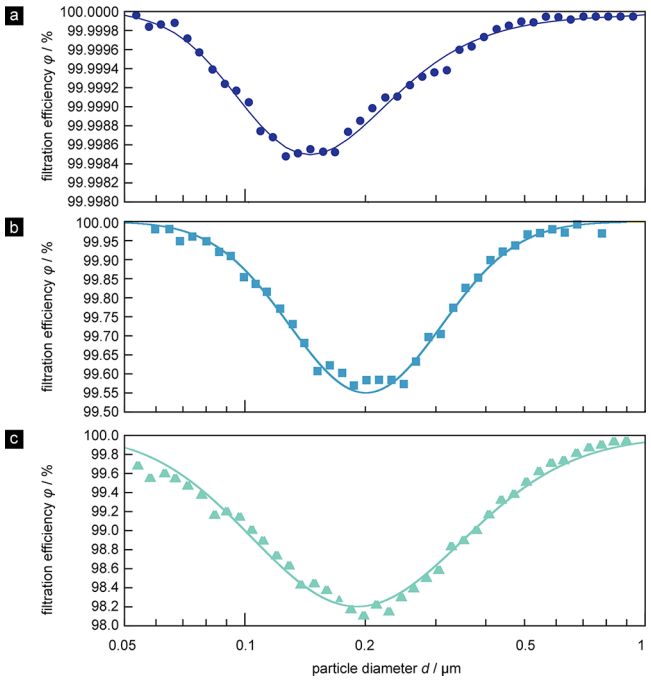

Figure 4. Particle filtration efficiency, φ, of NFAs with tailored porosity [93.91% (a), 96.64% (b), and 98.40% (c)] using a face velocity v_f of 1.5 cm s^{-1} and a particle loading of 29 mg m^{-3}. The data were fit according to the semiempirical filtration efficiency model by Lee and Liu.[58,60]

Table 1. Filtration Performance Measured at the MPPS with a Face Velocity of v_f = 1.5 cm s^{-1}[a]

porosity Φ (%)	filter efficiency φ (%)	pressure drop Δp (Pa)	fitted pore-wall thickness D_f (μm)	measured pore-wall thickness d_w (μm)	permeability κ ($\times 10^{-12}$ m^2)
93.91	99.998	550	1.40	2.7 ± 1.6	57.7 ± 01.1
96.64	99.56	115	2.01	5.5 ± 3.1	330 ± 18
98.40	98.2	60	4.22	7.8 ± 6.4	531 ± 17

[a]The effective wall thickness is compared with that indirectly measured via fit.

porosity of the nanofiber-based aerogel from 98.40 to 93.91%, the filtration efficiency was increased from 98.2% to reach 99.998%. In terms of permeated particles, this means an improvement by a factor of 1000. The most penetrating particle sizes (MPPSs) of the NFAs remain similar regardless of their porosities. This suggests an interception system and not a diffusion-limited system, like for other fiber-based filters. The pressure drop, however, increased at the same time from 60 to 550 Pa at a face velocity of v_f = 1.5 cm s^{-1} (Table 1). The interception parameter R in the model of Lee and Lui is related to the apparent fiber diameter, D_f, or, in the case of the aerogel, to the pore-wall thickness of the secondary cell like pores in the NFA. When the fit parameter D_f is compared with the experimentally measured pore-wall thickness, d_w, such a correlation is observed. Yet, the indirectly measured pore-wall thickness through the fitted filtration data is systematically lower (by a factor of approximately 2), indicating that the model by Lee and Lui cannot be used to fully approximate the filtration process within the NFAs with their hierarchical pore structure.

To further evaluate the filtration performance, a so-called quality factor (QF) can be calculated

$$\mathrm{QF} = -\frac{\ln(1-\varphi)}{\Delta p} \tag{5}$$

where φ is the filtration efficiency and Δp is the pressure drop.[62] Our NFAs had QFs between 0.020 and 0.096 Pa^{-1}. These values correspond well with the QF of electrospun[1,17,19,63,64] and melt-spun[1,2,65−67] nanofiber filters (0.01−0.001). Significant performance advantages of NFA filters compared to those of NFM filters are found in their dust-holding capacity and their tolerance of high face velocities, as shown in the following sections.

A linear dependence between the pressure drop and face velocity v_f was observed upon measurement of the face velocity

DOI: 10.1021/acsami.8b00455
ACS Appl. Mater. Interfaces 2018, 10, 9069−9076

as a function of the pressure drop (Figure S1). Assuming proportionality between v_f and the reciprocal height of the NFA, $1/L$, the effective permeability κ can be calculated according to the Hagen−Poiseuille equation[68]

$$v_f = -\frac{\kappa \Delta p}{\eta L} \quad (6)$$

where Δp is the pressure drop and η is the viscosity of air [η_{air}(25 °C) = 18.6 μPa s]. Depending on the porosity of the NFA, a permeability between 57.7×10^{-12} and 531×10^{-12} m^2 was found (Table 1).

3.3. Dust-Holding Capacity of NFA and NFM Filters. The performance of a filter as expressed by the QF may change significantly upon deposition of the first aerosol particles. This is in particular true for NFM filters, which offer a large free filtration area when clean but are rapidly filled with aerosol particles followed by cake formation on the surface of the filter.[69] Increased pressure drop and often reduced filtration efficiency[70] shorten the service life or require special cleaning cycles such as backpulsing and backblowing.[71,72] In contrast, the here-investigated NFA filters in contrast provide a large internal surface where particle adsorption should be dominated by deep-bed filtration without significantly affecting the hierarchical pore structure of the NFA. Figure 5 shows the

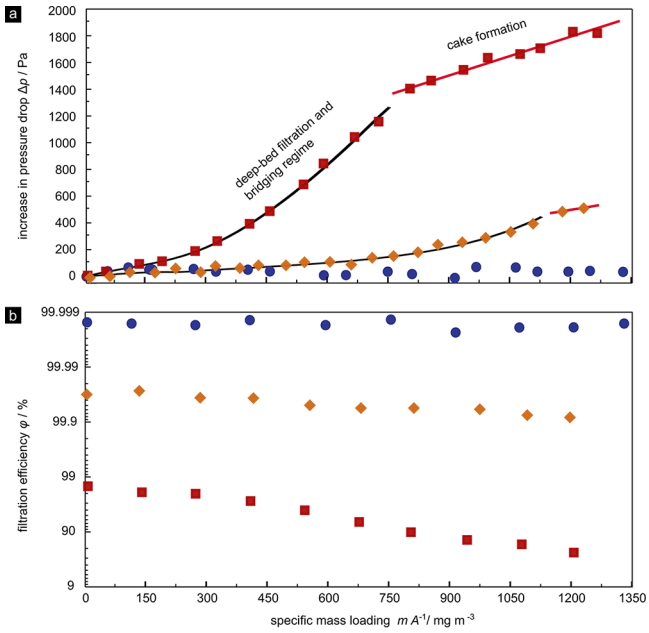

Figure 5. Long-term changes in the (a) pressure drop and (b) filtration efficiency at the MPPS with high aerosol particle loading. The NFA (blue ○) with a porosity of 93.91% showed neither a change in the filtration efficiency nor an increase in the pressure drop during the complete measurement cycle, whereas the commercial NFM filters with toppings (orange ◇) and without toppings (red □) showed a significant increase in the pressure drop due to bridging and cake formation. This, in turn, is locally increasing the face velocity at still open sites and thus decreasing the overall filtration efficiency.

long-term performance of our NFA filter compared with commercial NFM filters with and without toppings (123 ± 52 and 106 ± 37 nm mean fiber diameters; 1.0 and 1.2 g m^{-2} weight areas; for further characterization, see the Supporting Information). The NFM filter (Δp_{clean} = 324 Pa; QF = 0.013) shows the characteristic increase in the pressure drop with time with deep-bed filtration behavior at the beginning (capillary filling followed by binding, also referred to as the skin effect) with the transient to cake formation, where the pressure drop increases linearly with time.[69] This skin effect was also observed when the NFM was equipped with a topping of nonwoven microfibers (Δp_{clean} = 454 Pa; QF = 0.018), but it was less pronounced. This contrasts with the NFA filter that maintained its initial pressure drop (93.91% porosity; Δp_{clean} = 538 Pa; QF = 0.020) throughout the whole filtration experiment, even though bridging and cake formation will also happen at higher particle loadings. More importantly, the ultrahigh filtration efficiency of 99.998% at MPPS was maintained for the complete experiment (corresponding to more than 4×10^{11} aerosol particles), while the commercial NFMs showed an enormous decrease in their filtration efficiency from 99.97% to 99.91% for the NFM with topping and from 98.55% to 77.86% for the NFM without topping (Figure 5b).

3.4. Effect of the Face Velocity v_f on the Filtration Efficiency. The filtration efficiency of common electrospun thin NFMs depends not only on the dust loading but also on the face velocity.[13] Therefore, we investigated the dependence of the filtration efficiency on the face velocity. Figure 6 shows the typical behavior of NFA filters compared to a commercial NFM filter. For both filter types, the filtration efficiency drops with increasing face velocity and the MPPS moves to lower particle diameters. Both effects are well understood from filtration theory when taking into account that the diffusion particle capture mechanism, which is the dominating mechanism for the smaller particles, depends on the face velocity. However, the degree to which the filtration efficiency depends on the face velocity is very different for the NFA and NFM filters. When the face velocity increases from 0.75 to 6 cm s^{-1}, the three NFA filters with different porosities show a drop of the filtration efficiency by a factor of 1.5−10, whereas the commercial NFM filter showed a high efficiency drop from 99.99 to 98.95%, corresponding to a drop by a factor of 105 (Figure 7a). In a previous study, we investigated the dependence of the filtration efficiency on the pore architecture of the NFA.[26] Therefore, we produced NFAs with equal porosity but different sizes of the secondary pores from 15.2 to 122.6 μm diameter. The observed trends are very similar to those for the NFAs investigated before: a modest dependence of the filtration efficiency on the face velocity, which is more pronounced for the high efficiency NFA filters with smaller pores, underlining the importance of the diffusion particle capture mechanism for those filters (Figure 7b). The tolerance of NFA filters for high face velocities extends the design space for particle filters because the artificial enlargement of the inflow area, e.g., by pleating, is no longer mandatory.

4. CONCLUSIONS

NFAs show high particle filtration efficiency at a wide range of face velocities in combination with the ultrahigh dust-holding capacity. They have significant application potential in personal protection, clean-room and building management, as well as emission control. We studied the performance characteristics and morphological features of these filters and compared them with commercial electrospun NFM filters. We found that the number of permeated particles can be decreased by a factor of 1000 by simply tailoring the porosity of the NFA. By the introduction of a hierarchical open-pore structure into these 3D filtration media, diffusion captor was no longer the performance-limiting mechanism. Therefore, they show little depend-

DOI: 10.1021/acsami.8b00455
ACS Appl. Mater. Interfaces 2018, 10, 9069−9076

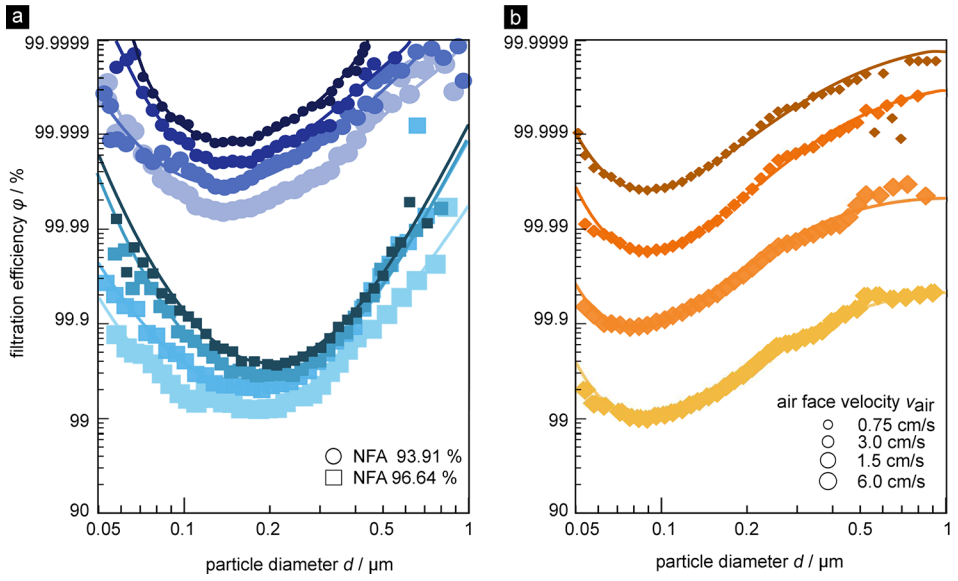

Figure 6. Effect of the face velocity on the filtration efficiency of (a) two NFA filters (violet ○ and blue □) and (b) a commercial NFM with topping (orange ◇). Increasing face velocities (0.75, 1.5, 3, and 6 cm s^{-1}) are indicated by the sizes of the symbols.

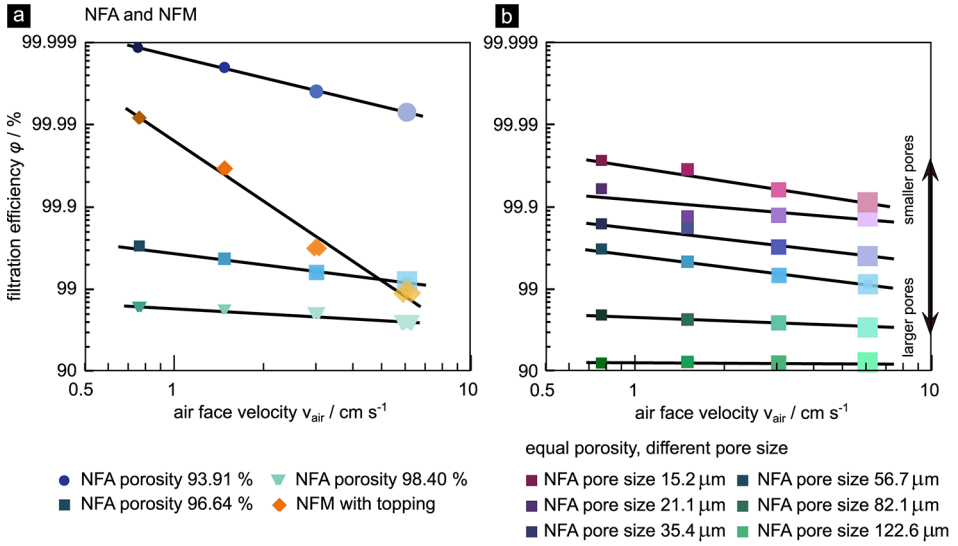

Figure 7. Effect of the face velocity (0.75, 1.5, 3, and 6 cm s^{-1}) on the filtration efficiency of NFA and NFM filters with (a) different porosities and (b) an equal porosity of 96.85% but different pore architectures with secondary pore diameters between 15.2 and 122.6 μm.

ence on the face velocity. Their superior capacity was demonstrated by long-term filtration tests with high particle loadings in which the NFA filters remained within the deep-bed filtration regime while NFM filters already showed cake formation with the need for a service interval or a dedicated cleaning procedure. Because the individual processing steps of these NFA filters are already employed in different industrial settings, we expect rapidly growing interest in such materials for filtration applications. Furthermore, considering the possibility of composite media consisting of NFAs and other materials, even a wider range of applications can be embraced.

■ ASSOCIATED CONTENT

Supporting Information

The Supporting Information is available free of charge on the ACS Publications website at DOI: 10.1021/acsami.8b00455.

Air permeability measurements, characterization of commercial NFMs, and particle-size distribution of DEHS test particles (PDF)

■ AUTHOR INFORMATION

Corresponding Author

*E-mail: christian.adlhart@zhaw.ch.

ORCID

Christian Adlhart: 0000-0002-4081-221X

Funding

This work was supported by Forschungsfond Aargau, TB-Safety, IVF-Hartmann AG (Thesis of F.D.), and COST Action MP1206 (traveling grants).

Notes

The authors declare no competing financial interest.

DOI: 10.1021/acsami.8b00455
ACS Appl. Mater. Interfaces 2018, 10, 9069−9076

REFERENCES

(1) Gopal, R.; Kaur, S.; Ma, Z.; Chan, C.; Ramakrishna, S.; Matsuura, T. Electrospun nanofibrous filtration membrane. *J. Membr. Sci.* **2006**, *281* (1−2), 581−586.

(2) Barhate, R.; Ramakrishna, S. Nanofibrous filtering media: Filtration problems and solutions from tiny materials. *J. Membr. Sci.* **2007**, *296* (1−2), 1−8.

(3) Shim, W. S.; Leea, D. W. Quality variables of meltblown submicron filter materials. *Indian J. Fibre Text. Res.* **2013**, *38* (2), 132−137.

(4) Ding, B.; Zhao, X.; Zhang, S.; Song, J.; Chen, K.; Yu, J. Anti-stripping electrospun nanofiber composite filter material with high abrasion resistance and its spinning method. Patent CN104028047A, 2014.

(5) Vinh, N. D.; Kim, H.-M. Electrospinning Fabrication and Performance Evaluation of Polyacrylonitrile Nanofiber for Air Filter Applications. *Appl. Sci.* **2016**, *6* (9), 235.

(6) Choi, H.-J.; Kumita, M.; Seto, T.; Inui, Y.; Bao, L.; Fujimoto, T.; Otani, Y. Effect of slip flow on pressure drop of nanofiber filters. *J. Aerosol Sci.* **2017**, *114*, 244−249.

(7) Si, Y.; Yu, J.; Tang, X.; Ge, J.; Ding, B. Ultralight nanofibre-assembled cellular aerogels with superelasticity and multifunctionality. *Nat. Commun.* **2014**, *5*, 5802.

(8) Teo, W. E.; Ramakrishna, S. A review on electrospinning design and nanofibre assemblies. *Nanotechnology* **2006**, *17* (14), R89−R106.

(9) Wendorff, J. H.; Agarwal, S.; Greiner, A. *Electrospinning: Materials, Processing, and Applications*; Wiley-VCH: Weinheim, Germany, 2012.

(10) Greiner, A.; Wendorff, J. H. Electrospinning: A Fascinating Method for the Preparation of Ultrathin Fibers. *Angew. Chem., Int. Ed.* **2007**, *46* (30), 5670−5703.

(11) Buttiker, R.; Ebert, J.; Hinderling, C.; Adlhart, C. Membranes for Specific Adsorption: Immobilizing Molecularly Imprinted Polymer Microspheres using Electrospun Nanofibers. *Chimia* **2011**, *65* (3), 182−186.

(12) Kirsh, A. A.; Stechkina, I. B.; Fuchs, N. A. Effect of gas slip on the pressure drop in a system of parallel cylinders at small reynolds numbers. *J. Colloid Interface Sci.* **1971**, *37* (2), 458−461.

(13) Xia, T.; Bian, Y.; Zhang, L.; Chen, C. Relationship between pressure drop and face velocity for electrospun nanofiber filters. *Energy and Buildings* **2018**, *158*, 987−999.

(14) Petrianov, I. V.; Sadovskii, B. F. Use of Petryanov-filter filtering materials in impactors. *Gig. Sanit.* **1973**, *38* (5), 74−76.

(15) Tucker, N.; Stanger, J. J.; Staiger, M. P. The History of the Science and Technology of Electrospinning from 1600 to 1995. *J. Eng. Fibers Fabr.* **2012**, *7*, 63−73.

(16) Sambaer, W.; Zatloukal, M.; Kimmer, D. 3D air filtration modeling for nanofiber based filters in the ultrafine particle size range. *Chem. Eng. Sci.* **2012**, *82* (C), 299−311.

(17) Sambaer, W.; Zatloukal, M.; Kimmer, D. 3D modeling of filtration process via polyurethane nanofiber based nonwoven filters prepared by electrospinning process. *Chem. Eng. Sci.* **2011**, *66* (4), 613−623.

(18) Li, P.; Wang, C.; Zhang, Y.; Wei, F. Air Filtration in the Free Molecular Flow Regime: A Review of High-Efficiency Particulate Air Filters Based on Carbon Nanotubes. *Small* **2014**, *10* (22), 4543−4561.

(19) Yang, Y.; Zhang, S.; Zhao, X.; Yu, J.; Ding, B. Sandwich structured polyamide-6/polyacrylonitrile nanonets/bead-on-string composite membrane for effective air filtration. *Sep. Purif. Technol.* **2015**, *152* (C), 14−22.

(20) Zhang, S.; Tang, N.; Cao, L.; Yin, X.; Yu, J.; Ding, B. Highly Integrated Polysulfone/polyacrylonitrile/polyamide-6 Air Filter for Multi-level Physical Sieving Airborne Particles. *ACS Appl. Mater. Interfaces* **2016**, *8* (42), 29062−29072.

(21) Wang, N.; Si, Y.; Wang, N.; Sun, G.; El-Newehy, M.; Al-Deyab, S. S.; Ding, B. Multilevel structured polyacrylonitrile/silica nanofibrous membranes for high-performance air filtration. *Sep. Purif. Technol.* **2014**, *126*, 44−51.

(22) Wang, N.; Yang, Y.; Al-Deyab, S. S.; El-Newehy, M.; Yu, J.; Ding, B. Ultra-light 3D nanofibre-nets binary structured nylon 6−polyacrylonitrile membranes for efficient filtration of fine particulate matter. *J. Mater. Chem. A* **2015**, *3*, 23946−23954.

(23) Zhang, S.; Liu, H.; Yin, X.; Yu, J.; Ding, B. Anti-deformed Polyacrylonitrile/Polysulfone Composite Membrane with Binary Structures for Effective Air Filtration. *ACS Appl. Mater. Interfaces* **2016**, *8* (12), 8086−8095.

(24) Leung, W. W.-F.; Hung, C.-H.; Yuen, P.-T. Effect of face velocity, nanofiber packing density and thickness on filtration performance of filters with nanofibers coated on a substrate. *Sep. Purif. Technol.* **2010**, *71* (1), 30−37.

(25) Deuber, F.; Mousavi, S.; Federer, L.; Adlhart, C. Amphiphilic Nanofiber-Based Aerogels for Selective Liquid Absorption from Electrospun Biopolymers. *Adv. Mater. Interfaces* **2017**, *4* (12), 1700065.

(26) Deuber, F.; Mousavi, S.; Hofer, M.; Adlhart, C. Tailoring Pore Structure of Ultralight Electrospun Sponges by Solid Templating. *ChemistrySelect* **2016**, *1* (18), 5595−5598.

(27) Duan, G.; Jiang, S.; Jérôme, V.; Wendorff, J. H.; Fathi, A.; Uhm, J.; Altstädt, V.; Herling, M.; Breu, J.; Freitag, R.; Agarwal, S.; Greiner, A. Ultralight, Soft Polymer Sponges by Self-Assembly of Short Electrospun Fibers in Colloidal Dispersions. *Adv. Funct. Mater.* **2015**, *25* (19), 2850−2856.

(28) Duan, G.; Koehn-Serrano, M.; Greiner, A. Highly efficient reusable sponge-type catalyst carriers based on short electrospun fibers. *Macromol. Rapid Commun.* **2017**, *38* (3), 1600511.

(29) Duan, G. G.; Jiang, S. H.; Moss, T.; Agarwal, S.; Greiner, A. Ultralight open cell polymer sponges with advanced properties by PPX CVD coating. *Polym. Chem.* **2016**, *7* (15), 2759−2764.

(30) Jiang, S.; Agarwal, S.; Greiner, A. Low-density open cellular sponges as functional materials. *Angew. Chem., Int. Ed.* **2017**, *56* (49), 15520−15538.

(31) Jiang, S.; Duan, G.; Kuhn, U.; Mörl, M.; Altstädt, V.; Yarin, A. L.; Greiner, A. Spongy Gels by a Top-Down Approach from Polymer Fibrous Sponges. *Angew. Chem., Int. Ed.* **2017**, *56* (12), 3285−3288.

(32) Jiang, S. H.; Uch, B.; Agarwal, S.; Greiner, A. Ultralight, Thermally Insulating, Compressible Polyimide Fiber Assembled Sponges. *ACS Appl. Mater. Interfaces* **2017**, *9* (37), 32308−32315.

(33) Si, Y.; Fu, Q.; Wang, X.; Zhu, J.; Yu, J.; Sun, G.; Ding, B. Superelastic and Superhydrophobic Nanofiber-Assembled Cellular Aerogels for Effective Separation of Oil/Water Emulsions. *ACS Nano* **2015**, *9* (4), 3791−3799.

(34) Si, Y.; Wang, X.; Yan, C.; Yang, L.; Yu, J.; Ding, B. Ultralight Biomass-Derived Carbonaceous Nanofibrous Aerogels with Superelasticity and High Pressure-Sensitivity. *Adv. Mater.* **2016**, *28* (43), 9512−9518.

(35) Stanger, J. J.; Tucker, N.; Buunk, N.; Truong, Y. B. A comparison of automated and manual techniques for measurement of electrospun fibre diameter. *Polym. Test.* **2014**, *40*, 4−12.

(36) Deuber, F.; Adlhart, C. Improved fiber diameter determination of nanofibers through image analysis using a hierarchical scaling approach. *NART 2015* **2015**, 29−36.

(37) Deuber, F.; Adlhart, C. From Short Electrospun Nanofibers to Ultralight Aerogels with Tunable Pore Structure. *Chimia* **2017**, *71* (4), 236−240.

(38) Huang, Y.; Lai, F.; Zhang, L.; Lu, H.; Miao, Y.-E.; Liu, T. Elastic Carbon Aerogels Reconstructed from Electrospun Nanofibers and Graphene as Three-Dimensional Networked Matrix for Efficient Energy Storage/Conversion. *Sci. Rep.* **2016**, *6*, 31541.

(39) Yu, Y.; Hua, S.; Yang, M.; Fu, Z.; Teng, S.; Niu, K.; Zhao, Q.; Yi, C. Fabrication and characterization of electrospinning/3D printing bone tissue engineering scaffold. *RSC Adv.* **2016**, *6* (112), 110557−110565.

(40) Lai, F.; Huang, Y.; Zuo, L.; Gu, H.; Miao, Y.-E.; Liu, T. Electrospun nanofiber-supported carbon aerogel as a versatile platform toward asymmetric supercapacitors. *J. Mater. Chem. A* **2016**, *4* (41), 15861−15869.

(41) Chen, W.; Chen, S.; Morsi, Y.; El-Hamshary, H.; El-Newhy, M.; Fan, C.; Mo, X. Superabsorbent 3D Scaffold Based on Electrospun

DOI: 10.1021/acsami.8b00455
ACS Appl. Mater. Interfaces 2018, 10, 9069−9076

Nanofibers for Cartilage Tissue Engineering. *ACS Appl. Mater. Interfaces* **2016**, *8* (37), 24415−24425.
(42) Kim, J. G.; Choi, T. J.; Chang, J. Y. Homogenized electrospun nanofiber reinforced microporous polymer sponge. *Chem. Eng. J.* **2016**, *306*, 242−250.
(43) Chen, W.; Ma, J.; Zhu, L.; Morsi, Y.; EI-Hamshary, H.; Al-Deyab, S. S.; Mo, X. Superelastic, superabsorbent and 3D nanofiber-assembled scaffold for tissue engineering. *Colloids Surf., B* **2016**, *142*, 165−172.
(44) Xu, T.; Miszuk, J. M.; Zhao, Y.; Sun, H.; Fong, H. Electrospun polycaprolactone 3D nanofibrous scaffold with interconnected and hierarchically structured pores for bone tissue engineering. *Adv. Healthcare Mater.* **2015**, *4* (15), 2238−2246.
(45) Duan, G.; Bagheri, A. R. R.; Jiang, S.; Golenser, J.; Agarwal, S.; Greiner, A. Exploration of macroporous polymeric sponges as drug carriers. *Biomacromolecules* **2017**, *18* (10), 3215−3221.
(46) Jiang, S.; Reich, S.; Uch, B.; Hu, P.; Agarwal, S.; Greiner, A. Exploration of the electrical conductivity of double network silver nanowires - polyimide porous low density compressible sponges. *ACS Appl. Mater. Interfaces* **2017**, *9* (39), 34286−34293.
(47) Xu, T.; Ding, Y.; Wang, Z.; Zhao, Y.; Wu, W.; Fong, H.; Zhu, Z. Three-dimensional and ultralight sponges with tunable conductivity assembled from electrospun nanofibers for highly sensitive tactile pressure sensor. *J. Mater. Chem. C* **2017**, *5*, 10288−10294.
(48) Xu, T.; Wang, Z.; Ding, Y.; Xu, W.; Wu, W.; Zhu, Z.; Fong, H. Ultralight electrospun cellulose sponge with super-high capacity on absorption of organic compounds. *Carbohydr. Polym.* **2018**, *179*, 164−172.
(49) Fukasawa, T.; Deng, Z. Y.; Ando, M.; Ohji, T.; Goto, Y. Pore structure of porous ceramics synthesized from water-based slurry by freeze-dry process. *J. Mater. Sci.* **2001**, *36* (10), 2523−2527.
(50) Araki, K.; Halloran, J. W. Porous Ceramic Bodies with Interconnected Pore Channels by a Novel Freeze Casting Technique. *J. Am. Ceram. Soc.* **2005**, *88* (5), 1108−1114.
(51) Shanti, N. O.; Araki, K.; Halloran, J. W. Particle Redistribution During Dendritic Solidification of Particle Suspensions. *J. Am. Ceram. Soc.* **2006**, *89* (8), 2444−2447.
(52) Deville, S.; Saiz, E.; Nalla, R. K.; Tomsia, A. P. Freezing as a path to build complex composites. *Science* **2006**, *311* (5760), 515−518.
(53) Deville, S. Freeze-Casting of Porous Ceramics: A Review of Current Achievements and Issues. *Adv. Eng. Mater.* **2008**, *10* (3), 155−169.
(54) Li, W. L.; Lu, K.; Walz, J. Y. Freeze casting of porous materials: review of critical factors in microstructure evolution. *Int. Mater. Rev.* **2012**, *57* (1), 37−60.
(55) Zhou, Y.; Fu, S.; Pu, Y.; Pan, S.; Ragauskas, A. J. Preparation of aligned porous chitin nanowhisker foams by directional freeze−casting technique. *Carbohydr. Polym.* **2014**, *112*, 277−283.
(56) Deville, S. The lure of ice-templating: Recent trends and opportunities for porous materials. *Scr. Mater.* **2018**, *147*, 119−124.
(57) Jiang, S.; Duan, G.; Schöbel, J.; Agarwal, S.; Greiner, A. Short electrospun polymeric nanofibers reinforced polyimide nanocomposites. *Compos. Sci. Technol.* **2013**, *88* (C), 57−61.
(58) Langner, M.; Greiner, A. Wet-Laid Meets Electrospinning: Nonwovens for Filtration Applications from Short Electrospun Polymer Nanofiber Dispersions. *Macromol. Rapid Commun.* **2016**, *37* (4), 351−355.
(59) Spurny, K. R. *Advances in aerosol filtration*; CRC Press/Lewis Publishers, 1998; p 533.
(60) Filatov, Y.; Budyka, A.; Kirichenko, V. *Electrospinning of micro and nanofibers: Fundamentals and application in separation and filtration processes*; Begell House Publishers, 2007; p 434.
(61) Lee, K. W.; Liu, B. Y. H. Theoretical Study of Aerosol Filtration by Fibrous Filters. *Aerosol Sci. Technol.* **1982**, *1* (2), 147−161.
(62) Stechkina, I. B.; Fuchs, N. A. Studies on fibrous aerosol filters - I. Calculation of diffusional deposition of aerosols in fibrous filters. *Ann. Occup. Hyg.* **1966**, *9* (2), 59−64.
(63) Hung, C.-H.; Leung, W. W.-F. Filtration of nano-aerosol using nanofiber filter under low Peclet number and transitional flow regime. *Sep. Purif. Technol.* **2011**, *79* (1), 34−42.
(64) Zhang, Y.; Yuan, S.; Feng, X.; Li, H.; Zhou, J.; Wang, B. Preparation of Nanofibrous Metal−Organic Framework Filters for Efficient Air Pollution Control. *J. Am. Chem. Soc.* **2016**, *138* (18), 5785−5788.
(65) Hassan, M. A.; Yeom, B. Y.; Wilkie, A.; Pourdeyhimi, B.; Khan, S. A. Fabrication of nanofiber meltblown membranes and their filtration properties. *J. Membr. Sci.* **2013**, *427* (C), 336−344.
(66) Patanaik, A.; Jacobs, V.; Anandjiwala, R. D. Performance evaluation of electrospun nanofibrous membrane. *J. Membr. Sci.* **2010**, *352* (1−2), 136−142.
(67) Zhang, Y. Z.; Lim, C. T.; Ramakrishna, S.; Huang, Z. M. Recent development of polymer nanofibers for biomedical and biotechnological applications. *J. Mater. Sci.: Mater. Med.* **2005**, *16* (10), 933−946.
(68) Sanjuan, M. A.; Muñoz-Martialay, R. Variability of the concrete air permeability coefficient with time. *Building and Environment* **1997**, *32* (1), 51−55.
(69) Leung, W. W.-F.; Choy, H.-F. Transition from depth to surface filtration for a low-skin effect filter subject to continuous loading of nano-aerosols. *Sep. Purif. Technol.* **2018**, *190*, 202−210.
(70) Jaroszczyk, T.; Petrik, S.; Donahue, K. Recent development in heavy duty engine air filtration and the role of nanofiber filter media. *Journal of KONES* **2009**, *16*, 207−216.
(71) Leung, W. W.-F.; Hau, C. W. Y. Skin layer in cyclic loading-cleaning of a nanofiber filter in filtering nano-aerosols. *Sep. Purif. Technol.* **2017**, *188*, 367−378.
(72) Leung, W. W.-F.; Hau, C. W.-Y. A model of backpulse and backblow cleaning of nanofiber filter loaded with nano-aerosols. *Sep. Purif. Technol.* **2016**, *169*, 171−178.

DOI: 10.1021/acsami.8b00455
ACS Appl. Mater. Interfaces 2018, 10, 9069−9076